Integrin-mediated adhesion as self-sustained waves of enzymatic activation

M. R. Block,[1,2] O. Destaing,[2] C. Petropoulos,[2] E. Planus,[2] C. Albigès-Rizo,[2] and B. Fourcade[2,3,*]
[1]*Chromatine and Epigenetics, Institut Albert Bonniot, INSERM-CNRS U823, 38042 Grenoble Cedex, France*
[2]*Dysad, Institut Albert Bonniot, INSERM-CNRS U823, Université Joseph Fourier, 38042 Grenoble Cedex, France*
[3]*Laboratoire Joliot Curie, CNRS Ens-Lyon, 46 allée d'Italie, 69364 Lyon Cedex 07, France*
(Received 27 January 2014; revised manuscript received 2 October 2014; published 6 October 2015)

Integrin receptors mediate interaction between the cellular actin-cytoskeleton and extracellular matrix. Based on their activation properties, we propose a reaction-diffusion model where the kinetics of the two-state receptors is modulated by their lipidic environment. This environment serves as an activator variable, while a second variable plays the role of a scaffold protein and controls the self-sustained activation of the receptors. Due to receptor diffusion which couples dynamically the activator and the inhibitor, our model connects major classes of reaction diffusion systems for excitable media. Spot and rosette solutions, characterized by receptor clustering into localized static or dynamic structures, are organized into a phase diagram. It is shown that diffusion and kinetics of receptors determines the dynamics and the stability of these structures. We discuss this model as a precursor model for cell signaling in the context of podosomes forming actoadhesive metastructures, and we study how generic signaling defects influence their organization.

DOI: 10.1103/PhysRevE.92.042704 PACS number(s): 87.17.Rt, 05.65.+b, 87.16.Xa, 87.17.Aa

I. INTRODUCTION

Cellular signal processing takes place through a sequence of patterning events in which initially homogeneous concentration fields differentiate in activation patterns coordinated in space and in time [1]. Examples of such out-of-equilibrium patterns are numerous in actin wave remodeling systems [2] and include, for example, dorsal ruffles [3] and podosomes [4–7]. In contrast to other actin structures, podosomes in Src-transformed cells are actoadhesive complexes [8] primary controlled by β_1 integrin receptor signaling [6] cycling between two conformational states [9]. Podosomes form in domains with intense phosphoinositide signaling [10,11], and they exhibit remarkable spatiotemporal metaorganization such as granulation of space by clusters of many individual podosomes, static or expanding annular ring called rosettes, or incomplete rosettes with spiraling shapes [12–17]. Cellular imaging shows these metastructures are dynamic. They can fragment, fuse, repel each other, or annihilate. Such patterns of activation are characteristic features of different classes of reaction-diffusion systems of the activator-inhibitor type [18,19] which describe localized out-of-equilibrium structures. An attractive problem is to relate these abstract systems serving as paradigms for pattern formation with key biochemical functional modules.

In what follows, we will mainly concentrate on rosette and spotlike solutions as generic solutions of a two-dimensional diffusion-reaction system. Localized solutions in excitable media such as spots or annular ring solutions have been studied in many very different problems related, for example, to signal propagation [19], actin waves [2,20–24], domain wall dynamics [25–27], and mathematical analysis of pattern formation due to chemical autocatalysis [28–32]. In addition to spatially localized solutions specific to large diffusion constant of the inhibitor compared to the activator, these models possess generally many other solutions [18,33,34] when the inhibitor and the activator have comparable diffusion lengths. This plethora of solutions, and how these systems bifurcate when parameters are sightly varied, render difficult comparison with experimental observations. In this paper, we will introduce a coupling mechanism related to receptor diffusion.

To keep the problem amenable to analysis, we will focus on signaling events which initiate pattern formations in podosome systems. Local changes in membrane composition with local increase of $PIP_2(4,5)$ concentration [35,36] coupled to receptor activation [9,37,38], to receptor recruitment and to $PIP_2(4,5)$ production [39,40] are known to regulate podosome structures [41]. By analogies with these mechanisms governing integrin signaling [42], we consider the model of Fig. 1; see also Ref. [43] for a different approach. We focus on a diffusing two-state receptor coupled to two functional modules. One is for receptor activation through concentration changes u in the membrane, while the other v plays the role of controller regulator. In the language of pattern formation, this concentration change u plays the role of the activator, while the so-called inhibitor v controls and regulates the production of u by binding to the receptors. Nonlinearities in our reaction-diffusion system, characteristic of different classes of systems describing localized excited states, appear naturally in the model through the kinetics between the conformational states of the receptors modulated by u. The key properties of this model are that receptor diffusion modulates the two-variable activator-inhibitor system by introducing a global coupling through a diffusing field. This leads to a crossover between different classes of models, limits the number of solutions, and is crucial for their stability when the controller variable is not necessarily long range with respect to the activator. Therefore, receptor diffusion is essential to get stationary structures with the property that they get smaller with excitability. As a result, both diffusion and kinetics properties of these receptors influence the stability of theses structures, their dynamics, and their response to local perturbations.

*bertrand.fourcade@ujf-grenoble.fr

 ©2015 American Physical Society

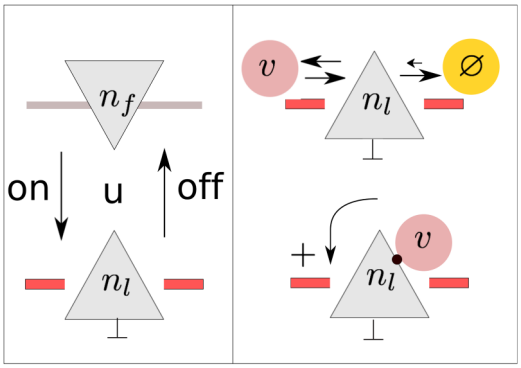

FIG. 1. (Color online) Schematic representation of the model. Left panel: Integrin receptors have two conformational states. Unactivated integrins are represented by down triangles and activated ones by up triangles. Changing membrane composition with increasing u as indicated by the color code of the bar drives integrin receptors from their unactivated to their activated state where they are immobilized by ligation to an extracellular ligand ($\perp$). Right panel: Activated integrins bind reversibly a controller protein represented as a pink circle with the symbol v. A covalent modification of v on the integrin site leads to the inert molecule $\varnothing$ represented as a yellow circle. Changes in affinity between integrins and v or $\varnothing$ are represented by right-left arrows. The complex $v \cdot n_l$ synthesizes u and thus favors the activated phase by a feedback loop.

II. THE MODEL

In the simplest case, an activator-inhibitor reaction-diffusion system takes on the form

$$\partial_t u = D_u \Delta u + f(u,v,n_l), \tag{1}$$

$$\partial_t v = D_v \Delta v + g(u,v,n_l), \tag{2}$$

where $u = u(x,t)$, $v = v(x,t)$, and $n_l(x,t)$ are local coverage functions of the space-time coordinates. Δ is the two-dimensional Laplacian, f, g are nonlinear functions depending on bifurcation parameters, and ϵ is a parameter which controls the excitability of the system. By definition, n_l is the fraction of activated receptors ligated to an external ligand. In standard two-variable models, n_l is a given function of u or v and enters as a functional parameter in the model. In marked contrast, n_l in the present work is a dynamic variable adjusting itself to u and v. As a result, the coupling between the activator and the controller variable depends on receptor diffusion biased by the production of u.

Let n_f be the fraction of unactivated receptors, free to diffuse within the membrane. First, we derive the equation of motion for (n_f, n_l). The kinetics between these two states controls the formation of adhesive complexes. Introducing the reaction rate constants $k_{\rm on}(u), k_{\rm off}(u)$ between the two populations $n_f(u), n_l(u)$, the equations of motion for the receptors are

$$\partial_t n_f = D_n \Delta n_f - k_{\rm on}(u) n_f + k_{\rm off}(u) n_l, \tag{3a}$$

$$\partial_t n_l = k_{\rm on}(u) n_f - k_{\rm off}(u) n_l. \tag{3b}$$

In general, adhesive complexes grow and stabilize for $k_{\rm on}(u) > k_{\rm off}(u)$. As seen later, the ratio $k_{\rm on}(u)/k_{\rm off}(u)$ can be interpreted as an affinity constant modulated by the membrane concentration u.

To derive the equations of motion (1) of the activator u and of the controller v, we consider the formation of the complex $v \cdot n_l$. For a general activator-inhibitor system, there is a positive feedback between v and u. This means that u is produced at a rate proportional to the complex $v \cdot n_l$, while it is degraded at a rate proportional to u. Therefore,

$$f(u,v,n_l) = \frac{1}{\epsilon}(-bu + v \cdot n_l), \tag{4}$$

where b and ϵ gives characteristic time scales. If the equilibrium between the complex $v \cdot n_l$ is sufficiently fast, the dimensional reduction $v \cdot n_l \propto v n_l$ gives the desired result, since v increases the rate of production of u.

Regulation of the spatial and temporal binding of the controller v is represented symbolically as

$$n_l(u) + v \underset{k_-}{\overset{k_+}{\rightleftharpoons}} v \cdot n_l(u) \xrightarrow{1/\tau} n_l(u) + \varnothing, \tag{5}$$

where $\varnothing$ corresponds to inert molecules and where the dots represent other intermediate states that we will neglect by concentrating on only one effective state. Equation (5) corresponds to a biologically pertinent case where covalent modifications of an adaptator protein occur on integrin sites and favor the disassembling of the adhesive structure. For simplicity, we assume in the last step of Eq. (5) that the unbinding rate is much larger that the binding rate so that the reverse step can be neglected.

Under general conditions, we can set $dv \cdot n_l(u)/dt = 0$ in (5). We find

$$v \cdot n_l = \frac{k_+}{k_- + 1/\tau} v n_l \tag{6}$$

and v has a positive feedback on u. The same stationary approximation shows that $-1/\tau v n_l$ couples u to v in the equation of motion of v. Thus, u is the negative feedback on v, since $n_l(u)$ increases with u. In general, the controller variable is also activated, and the most simple equation of v is obtained when v is in equilibrium with a reservoir of concentration v_c

$$g(u,v,n_l) = h(v_c - v) - 1/\tau v n_l, \tag{7}$$

where v is produced at a rate $h v_c$ to compensate its modification at a rate $-1/\tau v n_l$. Since τ sets the reference time scale, we set $\tau = 1$ and rescale the time coordinate in the equations of motion (1) for u and v to write

$$\partial_t u = D_u \Delta u + \frac{1}{\epsilon}[-bu + v n_l(u)], \tag{8}$$

$$\partial_t v = D_v \Delta v + h(v_c - v) - v n_l(u), \tag{9}$$

where, to keep the notations as simple as possible, ϵ as been redefined as

$$\frac{1}{\epsilon'} = \frac{k_+}{k_- + 1/\tau}\frac{\tau}{\epsilon} \tag{10}$$

with $\epsilon' = \epsilon$. By appropriate rescaling, the parameters b and h stands for $b(k_- + 1/\tau)/k_+$ and $h\tau$, respectively. Since $n_l(u)$ is known from (3), Eqs. (3), (8), and (9) form a closed system and generalize the classical two-variable activator-inhibitor system

to the case of receptors with two conformational states. As a first result, Eqs. (8) and (9) are of the general form (1) with ϵ being the ratio of a rate of production to the rate of regulation.

In the limit of small down-regulation, $\tau \gg 1$, Eq. (7) shows that the variations of the activator u are almost decoupled from the variations of v and one can take $v = v_c$ in (6). In this case, the equation of motion for u follows a variational principle. For $k_-\tau \ll 1$, it is not possible to write the equations of motions under a variational form. The smallness of the parameter τ represents, therefore, the departure from equilibrium. The dimensionless ratio $k_+\tau/\epsilon$ must, however, be sufficiently small to encode the strength of the activation process.

Equations (3a), (3b), (8), and (9) are general and do not depend on the exact functional form chosen for $k_{\rm on}(u)$, $k_{\rm off}(u)$. These are defined as follows. From Eq. (3), the relative fraction $n_l(u)/n_f(u)$ in the stationary limit is given by the ratio of the two kinetic constants $k_{\rm on}(u)/k_{\rm off}(u)$. We assume the simple ansatz

$$\frac{k_{\rm off}(u)}{k_{\rm on}(u)} = K_e^{-1} \exp\left[-\beta u/(1+u/c)\right] \tag{11}$$

with $K_e^{-1} = k_{\rm off}(0)/k_{\rm on}(0)$ The two constants β and c are positive, and the effect of $c > 0$ is to limit the fraction of activated integrins at large u. The constant c is not necessary for what follows but can be kept for generality. The choice of the exponential function in (11) is suggested by analogies with known thermodynamic principles for proteins. A differential shift in the chemical potential between the two conformational states influences the relative population of theses states. In our case, we assume that this shift depends on the concentration u with a factor $\beta > 0$ encoding the strength of the interaction between a receptor and its scaffold proteins. This ansatz is also consistent with Bell's law generally assumed to describe the life time of a bond subjected to a force [44].

Equation (11) determines $k_{\rm on}(u)$ and $k_{\rm off}(u)$ within a common multiplicative factor $\epsilon_{\rm int}$. This factor scales how fast or slow is integrin receptor kinetics. Stationary solutions depend only on the ratio $k_{\rm on}(u)/k_{\rm off}(u)$, and homogeneous solutions of Eqs. (3) depend only on the combination $k_{\rm on}(u) + k_{\rm off}(u)$. For simplicity, we define a reference scale parameter $\epsilon_{\rm int}$ and set:

$$k_{\rm on} = 1/\epsilon_{\rm int}, \tag{12}$$

$$k_{\rm off} = 1/\epsilon_{\rm int} K_e^{-1} \exp\left[-\beta u/(1+u/c)\right], \tag{13}$$

where c is some positive constant. Physically this choice corresponds to the case where a change in membrane concentration stabilizes the activated state and thus increases the time during which an immobilized receptor signals. Varying $\epsilon_{\rm int}$ changes the residence time of the receptors in their activated state as well as their diffusion length at constant ratio $k_{\rm off}/k_{\rm on}$.

Baseline values for the parameters area as follows [43,45]. For membrane proteins, Brownian diffusion constants are of the order of $D_n \approx 0.1\,\mu{\rm m}^2\,{\rm s}^{-1}$. The average integrin density is of the order of $1000\,\mu{\rm m}^{-2}$, and, due to their size ≈9–12 nm [46], their area coverage is much larger than the one of PIP_2 which is a low abundance phospholipid. A typical value of the base level of u is, therefore, of the order of 1%. We take the intrinsic on-rate of an integrin as $0.1\,{\rm s}^{-1}$ with an intrinsic off-rate of $10\,{\rm s}^{-1}$. This gives $K_e = 0.01$ with a characteristic surface coverage for excited regions of $u_c = 4.6\%$ when $\beta = 100$ and $n_\infty = 1$. Taking $b = 1$ and $\epsilon = 1$ gives a diffusion length for u on the order of 300 nm. The parameter $\alpha = \epsilon h/b$ gives the ratio of the characteristic times for the activator u and the controller v near their unperturbed values. Typical values for α used in this work give $\alpha < 1$, so that u respond faster than v, since regulation is slower than activation. Finally, mobile membrane proteins have almost equal diffusion constants. The ratio of the activator to the inhibitor diffusion lengths $\mu = (\epsilon h D_u/b D_v)^{1/2}$ is smaller than 1, but it is not infinitesimally small in contrast to standard activator-inhibitor systems [2,25,27,29].

III. TWO LIMIT CASES: FAST AND SLOW INTEGRIN ADAPTATION DYNAMIC

A. Equations of motion

To understand how this homogeneous state can be destabilized by local excited structures, it is instructive to consider first the limits of (a) slow and (b) fast reinforcement of the adhesive complex by integrin diffusion. For the sake clarity, the dimensionless parametrization of the model is introduced in Appendix A.

Case a corresponds to zero receptor diffusion and very fast receptor kinetics, $\epsilon_{\rm int} \ll 1$. Since integrin receptors do not diffuse, the total surface density of integrins can be considered as homogeneous and constant, $n_f + n_l = n_\infty$. Rescaling the spacial coordinates, we renormalize the diffusion constants with $d = D_v/D_u$. If integrin kinetics between the two states is fast enough, Eq. (3) gives $n_l(u) = k_{\rm on}(u)/k_{\rm off}(u) n_f(u)$.

The equations of motion for u and v become

$$\partial_t u = \Delta u + \frac{1}{\epsilon}[-bu + n_\infty v \Theta_a(u)], \tag{14}$$

$$\partial_t v = d\Delta v + h(v_c - v) - n_\infty v \Theta_a(u) \tag{15}$$

with

$$\Theta_a(u) = \frac{1}{1 + K_e^{-1} \exp\left[-\beta u/(1+u/c)\right]}. \tag{16}$$

If K_e depends on other factors such as mechanical stresses, we can Taylor expand (16) and recover the functional form studied in Ref. [23].

In case b, diffusion takes place instantaneously. The distribution of unactivated integrins is homogeneous and is fixed by the boundary conditions for n_f. We find $n_f = n_\infty/(1+K_e)$, where $K_e \approx K_e \exp[\beta u_h]$ for $u_h \ll 1$. In this case, the equations for u and v are

$$\partial_t u = \Delta u + \frac{1}{\epsilon}[-bu + n_0 v \Theta_b(u)], \tag{17}$$

$$\partial_t v = d\Delta v + h(v_c - v) - n_0 v \Theta_b(u), \tag{18}$$

where

$$\Theta_b(u) = \exp\left[+\beta u/(1+u/c)\right] \tag{19}$$

with

$$n_0 = \frac{K_e}{1+K_e} n_\infty. \tag{20}$$

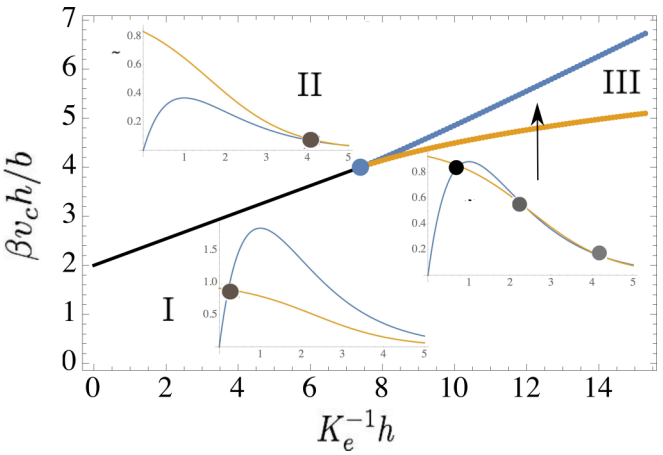

FIG. 2. (Color online) Parameter space in the limit of fast adaptation of the integrin field (b case). Typical null clines for regions I, II, and II are shown as insets. Region I, with one stable fixed point, corresponds to the monostable case studied in this paper. Solutions $u(t)$ and $v(t)$ in region II are oscillatory. In region III, the null clines correspond to a bistable system with three fixed points.

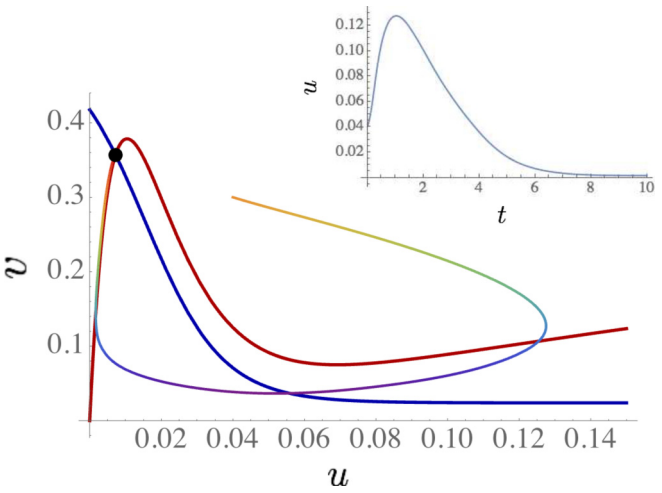

FIG. 3. (Color online) Generic trajectories (rainbow) in the (u,v) phase space with null clines (red, blue) in the case of slow adaptation of the integrin field (b case). The trajectory approaches the null cline $v = bu/n_l(u)$ (red curve) and u is bounded from above when $\epsilon \to 0$ before returning to the homogeneous fixed point. The inset shows the variations of $u(t)$ as a function of time ($h = 0.05, \epsilon = 1, b = 1$, $v_c = 0.5$).

Comparing the slow versus fast adaptive case shows that the equations of motions for u differ markedly, since the two functions $\Theta_a(u)$ and $\Theta_b(u)$ introduce very different nonlinearities and thus encode patterns with different properties. In the slow limit of case a, the dynamics of (14) corresponds to a cubic nonlinearity and the model is equivalent to a generalized FitzHugh-Nagumo model. In this case, ϵ sets the width of the interface between the rich and poor phases corresponding to the zeros of (14). In the fast adaptive limit, the equation of motion (17) has only two fixed points for $c = 0$ and three for $c > 0$. This model, for $c > 0$, has been first studied in Ref. [47], and we shall see that it has similar properties to autosolitons [25] with ϵ setting the width of the excited structures. Such structures have been thoroughly studied in Ref. [29] for the Gray-Scott model, which is approximately related to our model; see Appendix B.

In both cases, the controller variable v must be sufficiently large for the production of u by $v \cdot n_l(u)$, proportional to v, to compete with its irreversible degradation by the term $-bu$. As shown in Appendix A for the fast-adaptive case b, the ratio $\beta v_c h/b$ the relative contribution. On the other hand, activated receptor are down-regulated at rate 1 so that v must be constantly activated by $h(1-v)$ to maintain adhesive structures. As a result, the parameter space of Fig. 2 is the plane $(K_e^{-1}h, \beta v_c h/b)$ with one or three fixed points.

For parameters chosen in region III of Fig. 2, the system exhibits bistability, with two attracting points, with a low and a large (u,v) level, or the reverse, that essentially compete for the trajectory in the (u,v) plane. This region of the parameter space can describe alternate phases of fixed low and large u domains separated by domain walls with a width set by ϵ. In what follows, we will be primarily interested in the monostable case with only one fixed point (u_h, v_h); see region I. The reason for this is that, in contrast to region III, the homogeneous phase can be destabilized by local structure of arbitrary large u and low v for sufficiently small ϵ. In region II, the fixed point is still a stable focus when u_h is small and can generate a limit cycle through a supercritical Hopf bifurcation at larger values. For simplicity reasons, we will concentrate on region I.

B. Phase portrait analysis

To mark the difference between the two limits, it is useful to consider a phase portrait analysis of the equivalent two-variable system. The reduced system

$$du/dt = f(u,v), \tag{21}$$

$$dv/dt = g(u,v) \tag{22}$$

for (14)–(15) and (17)–(18) gives the null clines $v = u/n_l(u)$, $v = hv_c/[h + n_l(u)]$. As shown in Figs. 3 and 4, these null clines are very different in the two limits. In the slow adaptive case, $v = u/n_l(u)$ is S-shaped. We have $n_l(u) < n_\infty$ and $v \propto u$ in the large u limit. In the fast limit, however, the concentration of receptors increases very fast with the activator, and the null cline $v = u/n_l(u)$ decreases exponentially with u. Both systems are excitable, since a perturbation of the homogeneous fixed point triggers a strong excursion in the large u limit before returning the fixed point. For a large ensemble of parameters, this behavior is independent of the stationary approximation leading to (6).

The geometry of the null clines imposes, however, that cases a and b have very different behaviors as ϵ goes to zero. In case a, u is bounded from above as ϵ goes to zero, since the maximum value of u for a trajectory is where the null cline intersects a parallel to the u axis from the starting point. In case b, however, the null cline is almost parallel to the u axis, and the excitation u diverges in the same limit. This implies that the maximum of u can be made as large as desired by letting ϵ go to zero. As stated in Refs. [25,29], models for interfaces and domain walls dynamics fall generally in case a, but models for large self-sustained excitation spots correspond

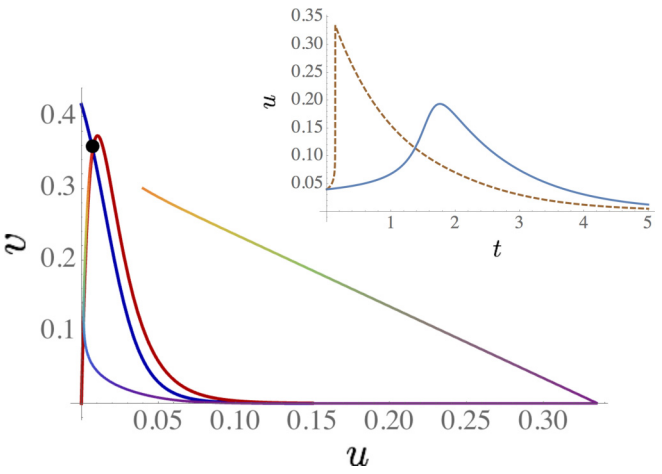

FIG. 4. (Color online) Generic trajectories (rainbow) in the (u,v) phase space with null clines (red, blue) in the extreme cases of instantaneous adaptation of the integrin field (b case). The inset shows the variations of $u(t)$ as a function of time in the cases where a constant c limit the production of u ($c \gg 1$, dashed, brown) and in the case where there is little saturation ($c = 0.1$, blue). Note that there is a strong separation of time scales between the fast increase of $u(t)$ and its slow return to the fixed point ($h = 0.05, \epsilon = 1, b = 1, v_c = 0.5$).

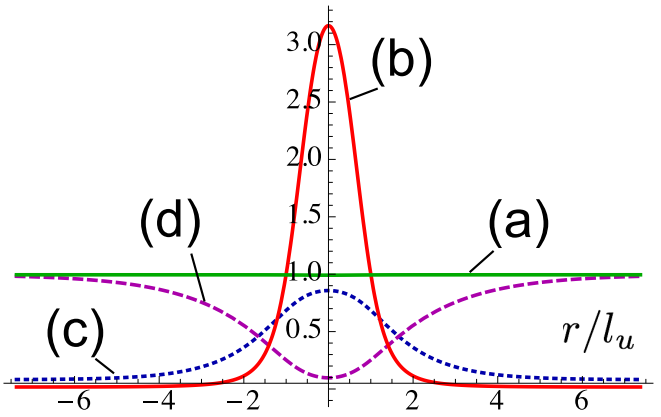

FIG. 5. (Color online) Example of a static spike obtained from a pointlike excitation. The density of free integrins (a) shown in green has almost converged to $n_\infty = 1$. Ligated integrins (b) are shown in red. The blue dotted line represents the variations of u (c) (normalized by its asymptotic value in one dimension; see (23). The dashed magenta line (d) corresponds to v/v_h. The distance r to the symmetry axis has been normalized by the diffusion length $l_u = \sqrt{D_u \epsilon / b}$ ($\approx l_v$) of u ($D_{u,v} = 1, h = 0.1, b = 2, v_c = 0.75, \epsilon = 5.75$). The scale where v varies is slightly larger than the characteristic scale of u with $l_u \lesssim l_v$.

to case b. Following Ref. [25], diffusion does not change this fundamental difference between the two limits, which will turn out to be essential to localize receptors.

IV. STATIC LOCALIZED STRUCTURES

On the numerical side, solutions are be obtained from the evolution of a pointlike excitation in u with fixed boundary conditions, all other fields being initially at their quiescent homogeneous state values. Following this initial condition, one observes a rapid adaptation of the dynamical variables with their eventual convergence to a stationary solution characterized by a constant density of unactivated receptors n_f. Nontrivial solutions, either stationary or not, are found for all values of the parameters near the I-II and I-III boundary lines of Fig. 2.

Figures 5 and 6 correspond to two generic stationary solutions with radial symmetry. These solutions are obtained in a regime where the pure kinetic case with $D_n = 0$ has only expanding ring solutions and where the limit $D_n \gg 1$ gives transient expanding solutions. Taking into account receptor diffusion is therefore crucial to obtain localized structures. Excited regions localized in the neighborhood of the maxima of u correspond to large concentration of receptors surrounded by a larger cloud with small concentration of the controller v. During convergence of the numerical solution, the receptors diffuse from the quiescent outside regions and get activated and immobilized where the density of ligated integrins is maximum. Numerically, immobilization of activated receptors is crucial for localized solutions to be stable. Otherwise, localized solutions fad away after their transient excitation.

Because 2D solutions can only be computed numerically, comparisons of our numerical results with the 1D solutions in the static case give useful trends. Assuming $d = D_u/D_v \ll 1$, the asymptotic analysis of Ref. [25] can be reproduced in our case and demonstrates that homoclinic orbits for $u(x)$ possesses a maximum u_{1d} [48]:

$$u_{1d} = 2/\sqrt{\pi}[dh/(b\epsilon)]^{1/2} v_h \tag{23}$$

on a characteristic length scale $l_u = \sqrt{D_u \epsilon / b}$, while $v(x)$ is a minimum in the spike and behaves exponentially outside on a characteristic length scale $l_v = \sqrt{D_v / h}$. Since $n_l(x)$ behaves as a delta in (18), the distribution of $v(x)$ is also exponential in two dimensions. This calculation shows that localized solutions in our model behave as autosolitons [25] with a maximum which increases and a characteristic spatial length scale which decreases as ϵ approaches zero.

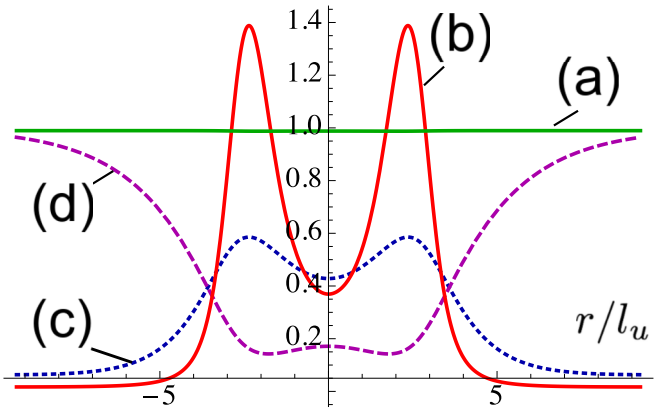

FIG. 6. (Color online) Example of a static radially symmetric rosette obtained from a pointlike excitation. Compared with the solution of Fig. 5, the excitability parameter ϵ is slightly decreased so that the the solution has the shape of a radially symmetric rosette ($D_{u,v} = 1, h = 0.1, b = 2, v_c = 0.75, \epsilon = 3.65$). The color code is the same as in Fig. 5: (a) n_f, (b) n_l, (c) u/u_{1d}, (d) v/v_h.

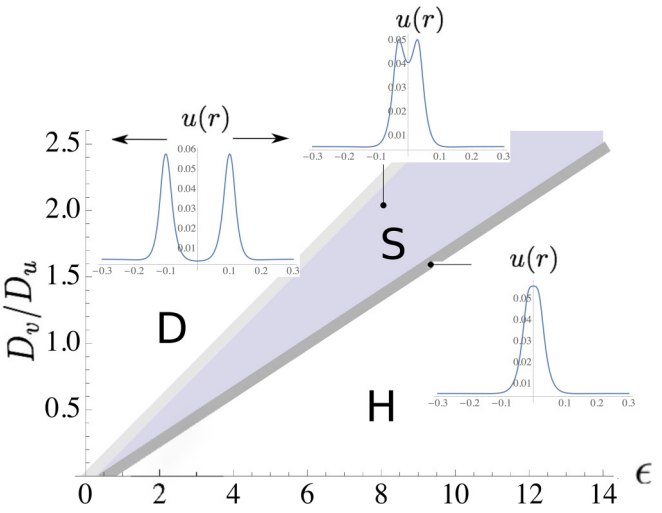

FIG. 7. (Color online) Phase diagram for 2D localized structures (case b with $c = 0$). D, S, and H correspond to nonstationary (expanding rosettes), static (stable), and homogeneous solutions. The insets show snapshots of $u(x)$. From left to right: Radially symmetric expanding rosettes, static rosettes near the left boundary line D-S, spike near the right boundary line S-H. Nonstationary solutions exist only on the left of the D-S line. Static solutions are obtained after convergence of the integrin field to 1 ($h = 0.1, b = 2, v_c = 0.75$). Note that expanding rings can be unstable and fragment in the vicinity of the D-S line as shown in Fig. 12. Dashed lines have been traced by hand.

Typical phase diagrams in the $(\epsilon, D_v/D_u)$ plane are presented in Figs. 7 and 8 and, to be more general, in Fig. 10. They correspond to different sets of parameters $\beta v_c h/b$ and $K_e^{-1}h$ of Fig. 2 and are generic for region I. As a general rule,

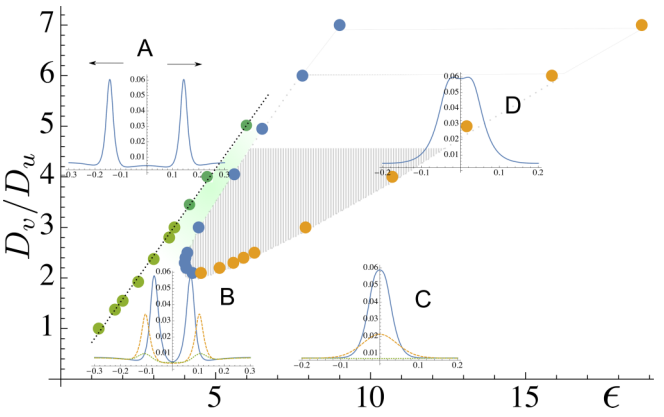

FIG. 8. (Color online) Phase diagram in the small $\beta h v_c/b$ limit ($h = 0.05, v_c = 0.5, b = 1$). The shaded area corresponds to the domain of stationary localized solutions (inset D). This domain is bounded from below by a minimum value of the diffusion constant D_v below which stationary solutions cannot be found. Only transient spikes fading away can be excited on the down right side of the shaded area (inset C). Going left from inset C to inset B, only transient expanding rings can be excited. Between the shaded area and the left dotted line traced by hand, the only solutions found are expanding rings which rapidly fragment into self-replicating spots as in Fig. 12 for a wide range of integrin diffusion constants. On the left of this dotted line, we find stable radially symmetric expanding rosettes.

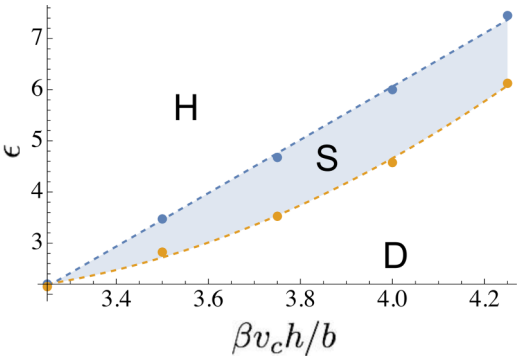

FIG. 9. (Color online) Values of ϵ at the S-D (ϵ_{sd}, lower curve) and at the H-S boundary line (ϵ_{hs}, upper curve) at fixed $d = D_v/D_u = 1$. Static solutions exist only in the colored region. The width of this region, $\epsilon_{sd} - \epsilon_{hs}$, decreases with v_c when $\beta v_c h/b$ approaches a critical value below which no localized solution exists ($h = 0.1, b = 2$).

moving from the left to the right hand side of the parameter space of Fig. 2 at D_v/D_u constant decreases the characteristic length for the spatial variations of the controller v with respect to the activator u. All phase diagrams exhibit the same generic topology with a domain of existence of stationary solutions. This domain is bounded on the right-hand side along the stationary-homogeneous line (S-H line), for large ϵ, by the trivial homogeneous phase and on the left-hand side, for small ϵ, by nonstationary solutions, such as expanding rosettes, along the dynamic-stationary line (D-S line). As shown in the insets of the first phase diagram, stationary solutions of the PDE system (3) and (8) near the S-H line have the shape of a single radially symmetric spike, but solutions near the D-S boundary line are rosettes with axial symmetry.

Stationary solutions exist if the rate of irreversible regulation of v is exactly compensated by the diffusion of v. Physically the problem is equivalent to the classical problem of equilibrating the rate of supply of the substance v with the rate of consumption of v in the excited regions. This rate depends on the excitability parameter ϵ fixing the rate of production of u. Integrin receptors are recruited through the increase of the

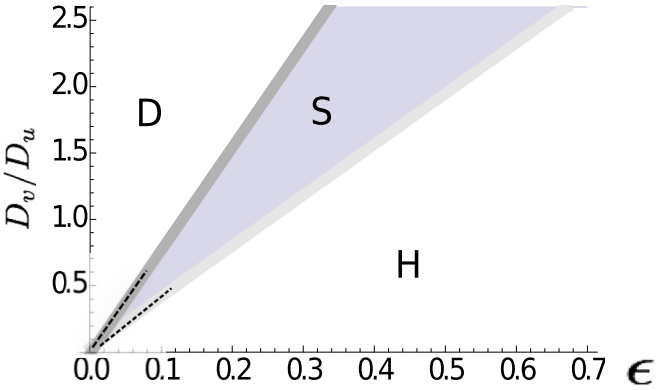

FIG. 10. (Color online) Example of a phase diagram for $c > 0$ in (11). Taking $c > 0$ limits the relative fraction of activated receptors which saturates for large u. Comparing with the phase diagram of Fig. 7, all phases are shifted to lower excitability parameter ϵ, but the general topology is unchanged ($h = 0.44, b = 2, c = 0.05$).

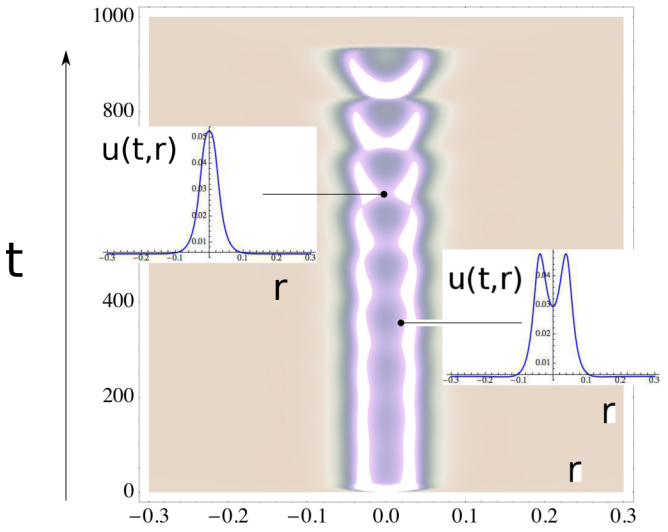

FIG. 11. (Color online) Density plot for u when an radially symmetric rosette experiences breathing oscillations near the D-S bifurcation line. The shape oscillates with time between the two shapes shown in the insets. For the values of the parameters used in this simulation ($D_v = D_u = 0.5D_n = 1$, $c = 25$), the D-S and the S-H bifurcation points almost coincide and the shape finally collapses.

production of u with ϵ and, in turn, this rate determines the rate of consumption of v via the product $vn_l(u)$. The shape of the excited domains depends on the spatial distribution of integrin receptors. Since these are recruited from the homogeneous phase through diffusion, they prefer to localize at the periphery of the rosette which expands as ϵ decreases. In the same way, increasing the diffusion constant D_v of v at fixed ϵ increases the rate of consumption of v which can only be achieved by recruiting new receptors at the periphery.

The rate of supply of v depends not only on the diffusion constant D_v but also on how v is produced from a reservoir at concentration v_c and at rate h. When the parameter hv_c/b is small, diffusion of v is not always able to maintain stationary localized structures. Figure 8 shows a phase diagram for smaller h. The domain where stationary localized solutions are found does not extend to small ratio D_v/D_u. This shows that the diffusion constant D_v should be large enough to obtain stationary solutions. The role of this diffusion constant can be better understood in the $(\beta v_c h/b, \epsilon)$ plane at fixed ratio D_v/D_u. When D_v is fixed and for a given hv_c/b, the domain for static stationary solutions is an interval for ϵ from a minimum value, ϵ_{sd}, corresponding the static-dynamic boundary line, to a maximum value, ϵ_{hs}, corresponding to the static-homogeneous boundary line. As done in Fig. 9, decreasing v_c at fixed h and D_v measures the width of the interval, $\epsilon_{hs} - \epsilon_{sd}$, where stationary solutions are found as one goes down parallel to the $\beta h v_c/b$ axis of Fig. 2. In this plane, the domain of existence of stationary solution has the shape of a tongue ending at a point below which no stationary solution can be found. This

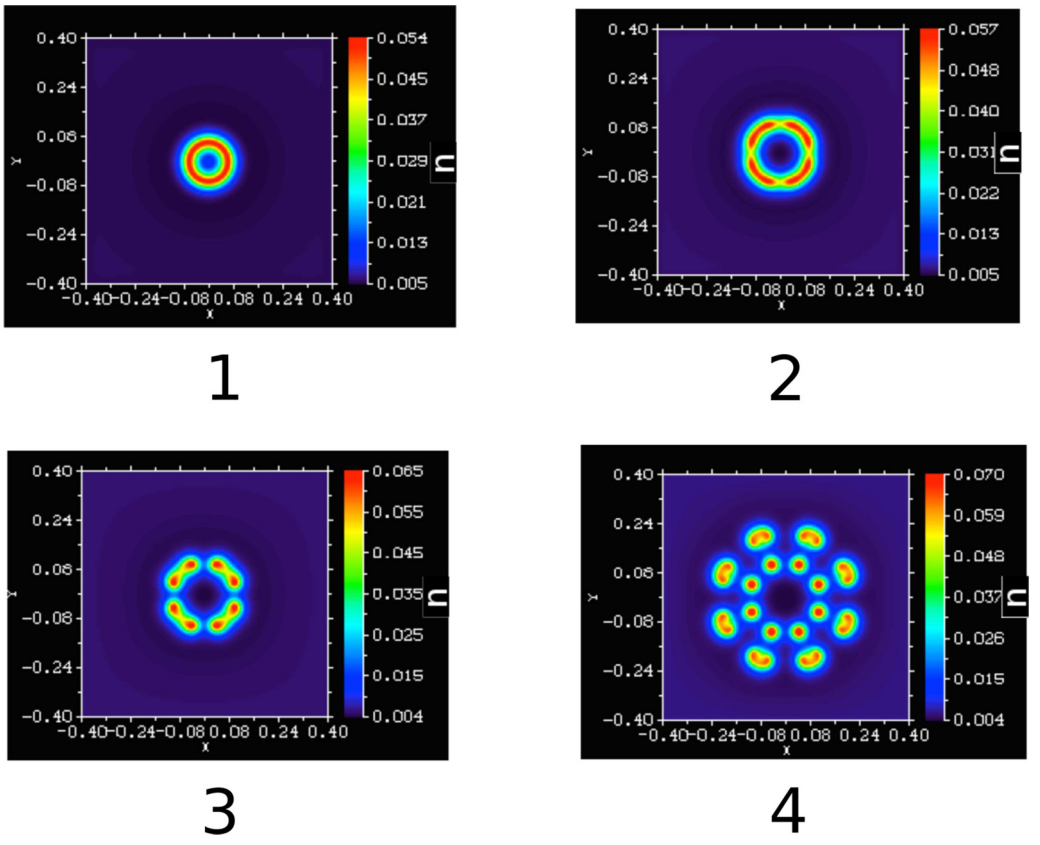

FIG. 12. (Color online) Density plots of the activator u at successive times for an expanding rosette when parameters are chosen on the left-hand side vicinity of the D-S boundary line of Fig. 7 ($\epsilon = 3.50$, $D_v/D_u = 1.0, D_n = 2$). The rosette starts expanding with radial symmetry in 1 and thereafter fragments into self-replicating spots in panels 2, 3, and 4. For larger integrin diffusion constant, $D_n = 10D_u$, the radially symmetric rosette is stable. In this case, it stops expanding due to boundary conditions and adopts a square shape.

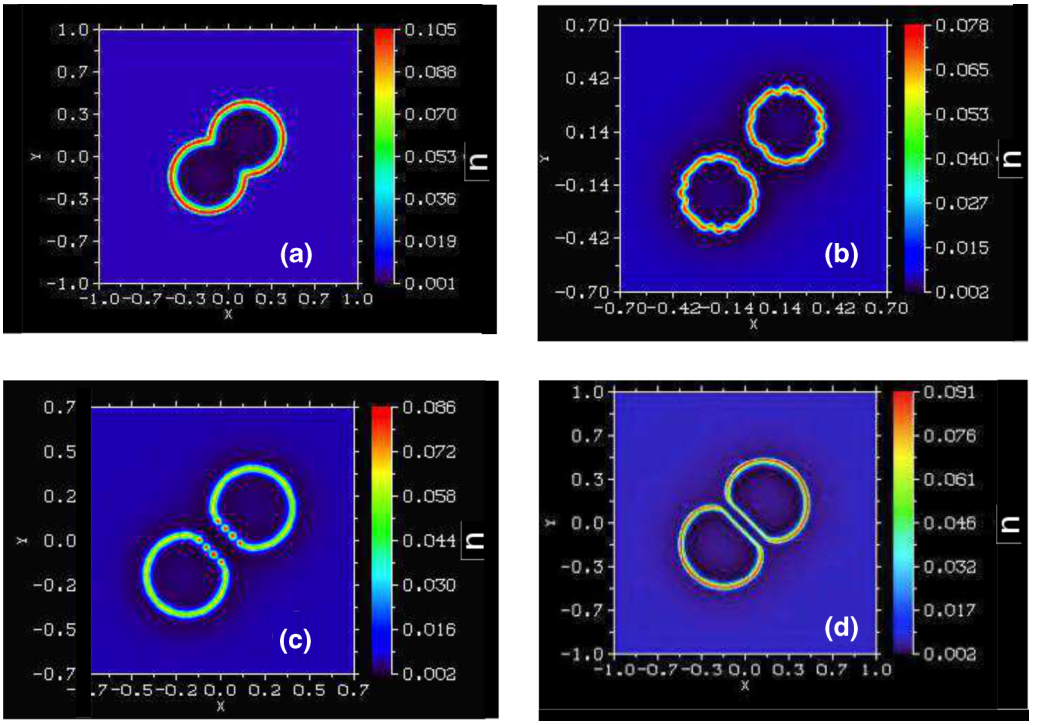

FIG. 13. (Color online) Density plots of the activator u. A collision between two expanding rosettes induces four characteristic different shape instabilities depending on receptor kinetics and diffusion constant. Case (a) is an annihilation of rosettes which initially expanded in the kinetic dominant regime where the recruitment of integrin receptors is small ($D_u = D_v = D_n, \epsilon_{\text{int}} = 0.5, \epsilon = 0.5$). Scaling down both k_{on} and k_{off} induces a zig-zag instability in case (b) followed by budding of self-replicating small spots granulating the space, $\epsilon_{\text{int}} = 0.7$. For different excitation, $\epsilon = 1$, and faster receptor kinetics, $\epsilon_{\text{int}} = 0.15$, the rosettes exhibit in case (c) a pearling instability which propagates from the point of contact between the two rosettes. For much larger diffusion length of the receptors, $D_n = 10 D_{u,v}, \epsilon = 1, \epsilon_{\text{int}} = 1$, the two rosettes repel each other without fusing or splitting into spots ($h = 0.05, b = 1, v_c = 0.5$).

point defines a minimum value of v_c which decreases with increasing D_v. We conclude that for each value of diffusion coefficient D_v, there exists a critical value of the parameter $\beta h v_c / b$ where no stationary solutions can be found. Similar conclusions apply for more complicated models such as the one of Fig. 10 for which the constant c in (11) is such that $k_{\text{off}}(u)$ saturates at large u ($c > 0$).

Finally, oscillating structures are found in the immediate vicinity of the D-S line. Figure 11 is an example of a fluctuating radially symmetric rosette exhibiting breathing deformations and collapsing after a few periods. These oscillations indicate that static rosettes are destabilized through a breathing mode when the excitability parameter ϵ is decreased.

V. EXPANDING ROSETTES, INSTABILITY TOWARDS GRANULATION OF SPACE, AND SPIRALING ROSETTES

A. Large inhibitor diffusion length ($l_v \gtrsim l_u$)

On the left-hand side of the D-S line, one finds expanding rosettes. When the diffusion length of v is slightly larger than the one of u, the dynamics of the integrin receptors is crucial and determines how receptors are distributed. For fast

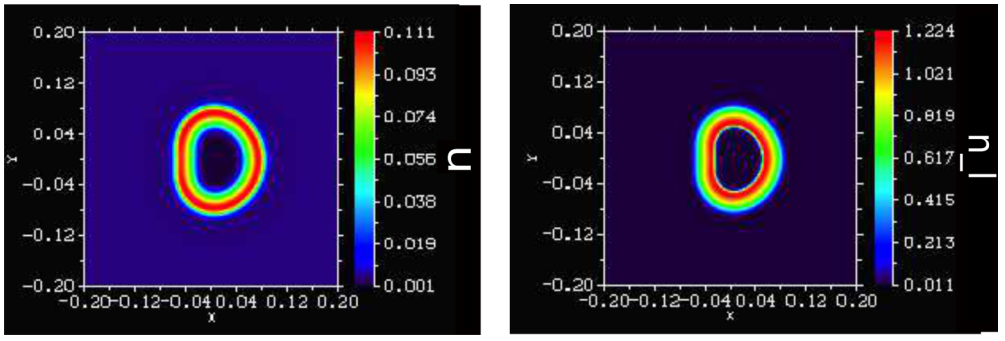

FIG. 14. (Color online) Expanding rosette in the case of a small controller diffusion length. The left panel represents the density map for the activator u. The right panel is for ligated integrin receptors n_l. Starting with a noncircular initial condition the rosette recovers asymptotically a radially symmetrical shape. As shown by comparison between the figures, this regime is characterized by strong gradients in signaling components across the rosette, n_l being maximal at the intrados.

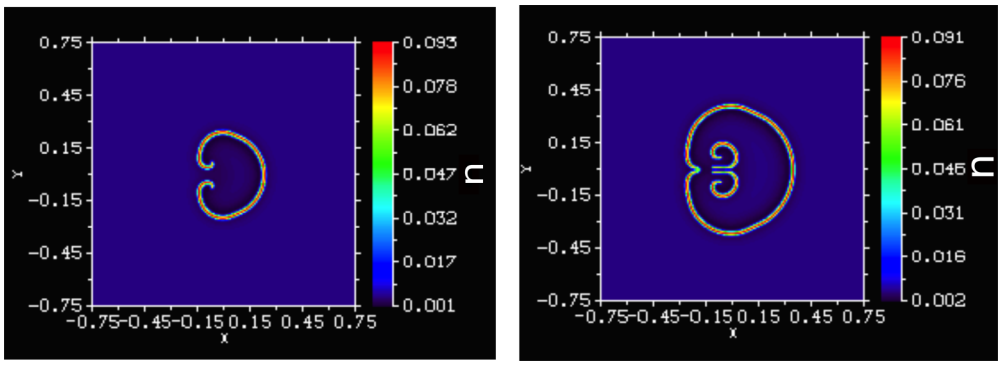

FIG. 15. (Color online) Density map of the activator u when the activator and the controller variable have comparable diffusion lengths. The two panels correspond to successive snapshots of spiral waves. Starting from a noncircular initial condition, the rosette started expanding to recover a circular shape. At later time, a dynamic ablation defect was numerically simulated by stetting the concentration fields of integrin receptors to zero in a small spot. Subsequent diffusion of integrin receptors towards this spot immediately destabilized the rosette, and the tip started to trace an involute shape (left panel). As shown in Fig. 16, the tips of the spirals are highly excited regions. They recover by fusion and expel receptors in excess to an inside double spiral (right panel). The outside rosette started again to expand while the inside spirals circle around their core ($h = 0.1, b = 1, D_u = D_n, D_v = 0.1 D_u, \epsilon = 0.1$).

kinetics, i.e., large $k_{\text{on,off}}$ with ϵ_{int} sufficiently small, solutions are characterized by a large density of activated receptors binding at the extrados of the rosette. On the other hand, for smaller kinetics with larger ϵ_{int}, both the density of ligated integrins and the radial speed decrease. In general, increasing the integrin diffusion constant D_n increases the radial speed, and, during expansion, this speed decreases with curvature.

Depending on the receptor kinetics, rosettes can expand radially or split into spots which later self-replicate and fill the space. Figure 12 is an example of a solution which started expanding with radial symmetry and breaks into spots above a given radius; see Ref. [49] for digital movies. Such solutions are also observed on the left of the D-S boundary line of Fig. 8 and are common when the initial point like excitation for u deviates sufficiently from a circular shape. For $D_v \geqslant D_u$ and larger excitability, i.e., smaller ϵ, rosettes expand with radial symmetry for slight perturbation of the circular initial excitation spot.

Still in the regime where the diffusion length is larger that the one of the activator, receptor diffusion and kinetics determine how solutions are sensitive to boundary conditions. As shown in Fig. 13, this parameter governs the shape evolution of expanding rosettes as they come into contact. Depending on integrin dynamics, four scenarios are possible. When the receptor diffusion constant is small, the two rosettes annihilate each other and form a unique expanding rosette with asymptotic radial symmetry (case a). This annihilation property is generally presented as the signature of excitable systems, as first demonstrated in Ref. [47]. In the intermediate regime, where the receptor diffusion length is comparable but larger than the controller diffusion length, D_v, the rosettes stop expanding at some distance and stay almost circular for a long time. This pause in expansion is followed by a slow adaptation of the integrin field, which, in turn, perturbs the rosettes out of their circular shape. Two cases are possible. In case b, one observes a zig-zag instability along the entire rosette followed by budding of spots towards the interior and the exterior of the rosettes. For case c, however, starting from the contact zone, the rosette breaks step by step into spots which granulate the space though self-replication as in case 4 of Fig. 12. In case d, the diffusion constant for interns is much larger than D_v. The two rosettes deform and form two parallel lines while expanding. Because calculations are necessarily done on a finite domain, we cannot assert that no granulation of space takes place in this case, but they have not been observed for different systems sizes.

B. Small inhibitor diffusion length ($l_v \lesssim l_u$)

For smaller inhibitor diffusion length, one enters a different regime. In this limit, rosettes expand and become asymptotically circular even if the initial condition deviates strongly from a circular spot. This regime is characterized by strong gradients in signaling components (see Fig. 14) and by annihilation of rosettes as in case a of Fig. 13. As before, expanding rosettes can be strongly perturbed by defects. As

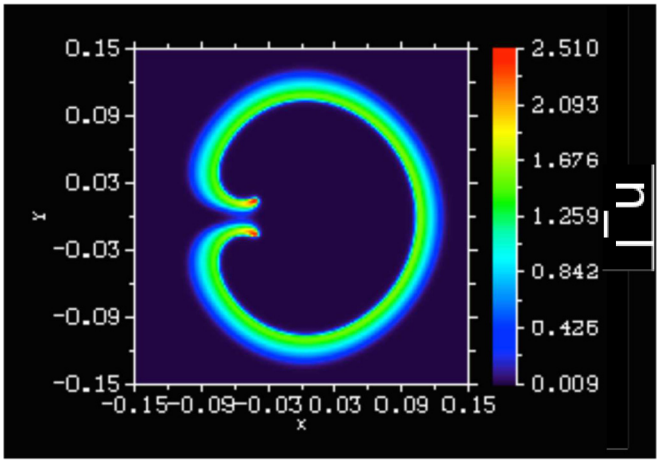

FIG. 16. (Color online) Distribution of ligated integrin receptors in the spiral wave of Fig. 15. The tips of the spirals having small curvature radii are the most excited regions where receptors concentrate. Note that ligated integrins are preferentially concentrated in the intrados of the rosette in the outside circular regions.

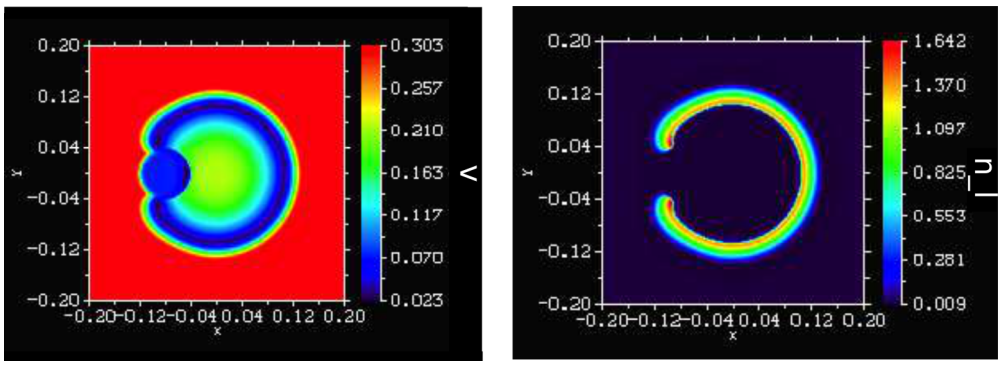

FIG. 17. (Color online) Density map of the controller v, left panel, and of the density of ligated integrins, n_l, for an expanding rosette colliding with a defect. The defect is simulated by taking $v_c = 0$ inside the left blue circle, so that v cannot be activated within the circle. While expanding, the rosette encircles the defect at right angle as shown in the right panel for the distributions of ligated integrins. The rosette will resume asymptotically its circular shape after passing over the defect and fusing the two arms together. Parameters are those of Fig. 15.

an example, Fig. 15 represents the evolution of a nonradially expanding rosette perturbed by numerical depletion of integrins within a spot in the course of the simulation. Mimicking optogenetic methods for light stimulated ablation of integrins [15], we set $n_l = 0$ in a small localized spot and let the integrin field adjust itself dynamically afterward. The shape dynamics is sensitive to this perturbation and traces a spiral which is usually interpreted as a characteristic feature of a slow short-range inhibitor. The curvature at the tip of the spirals being small, the excitation in this region is very strong with a large concentration of receptors; see Fig. 16. In all simulations, the rosette recovers its circular shape by fusing lines of excited domains and expelling an excess of activated receptors forming two spirals in the inside.

Other defects in signaling can be simulated in the same way. Since the controller v is activated from v_c through the term $h(v_c - v)$ in the equation of motion of v, one can also pattern the space to make v_c space dependent. Figure 17 is an example of an expanding rosette colliding with a circular defect where $v_c = 0$ inside a spot. While the rosette is still expanding, the defect breaks the circular symmetry all along the rosette, the rosette encircles the defect at right angle as the involute of a circle and resumes asymptotically its circular shape.

VI. STOCHASTIC SIMULATIONS

The stability of static and dynamic structures can be studied using the stochastic version in the 2D simulation. To mimic the effects of a number of chemical reactions which have been neglected so far in the model, we have studied the following model where $\eta_{l,f}(x,t)$, $\eta_v(x,t)$,$\eta_u(x,t)$ are random Gaussian variables uncorrelated in space and in time with variance R_n, R_u, R_v:

$$\partial_t n_f = D_n \Delta n_f - k_{\rm on}(u) n_f + k_{\rm off}(u) n_l + 1/\tau_n (n_r - n_f) + \eta_f(x,t), \quad (24)$$

$$\partial_t n_l = k_{\rm on}(u) n_f - k_{\rm off}(u) n_l + \eta_l(x,t), \quad (25)$$

$$\partial_t u = D_u \Delta u + \frac{1}{\epsilon}\{-b[1+\eta_u(x,t)]u + v n_l(u)\}, \quad (26)$$

$$\partial_t v = D_v \Delta v + h(v_c - v) - v n_l(u) + \eta_v(x,t). \quad (27)$$

The first equation introduces a reservoir of density n_r for unbound integrins and mimics random cellular integrin traffic. The second adds a stochastic noise for bound integrins. This term can be scaled by the product $n_l(u)v$ and adding a stochastic noise mimics the general interaction of bound integrins

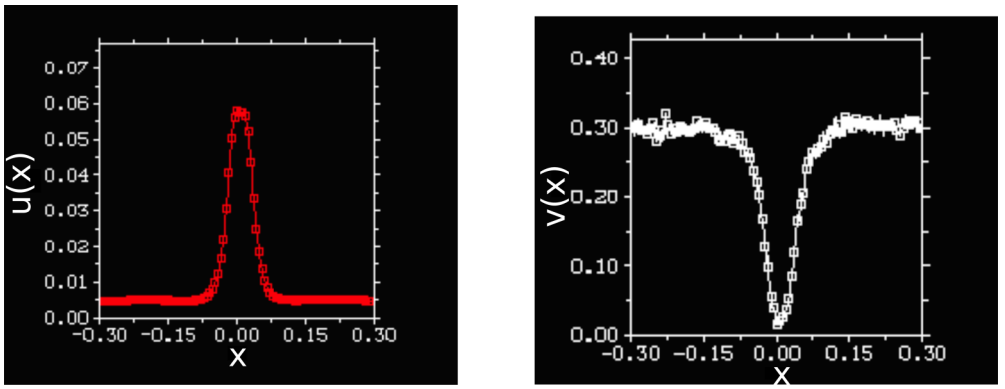

FIG. 18. (Color online) Cut of $u(x,y)$ and $v(x,y)$ along the the $y = 0$ axis for a $2-d$ fluctuating spike for $R_n = R_u = R_v = 1$ in Eq. (24). Despite the strong fluctuations, the shape of the spike fluctuates around its mean position without breaking into multiple spots, $\epsilon = 2$, $h = 0.1$, $v_c = 0.35$, $1/\tau_n = 0.1$).

with their environment. The third and fourth equations are equivalent to the previous model but with random b and v_c terms. Even for $R_n = R_u = R_v = O(1)$, we find that static structures are remarkably stable and fluctuate in time when they have the shape of a spike see Fig. 18. Static rosettes with a centered minimum, however, tend to break and to form moving interacting fragments and self-replicating spots.

VII. DISCUSSION AND CONCLUSION

In comparison with other existing models for cellular signaling waves, our model takes into account the effect of receptor diffusion for an activator-inhibitor model. Its aim is to describe in a minimal way signaling events as precursors of actoadhesive structures. Receptor diffusion modulates the coupling between the activator and the inhibitor field in an other way than the spatial averaged coupling studied before see Ref. [28]. It allows one to crossover from front solutions to pulse solutions in excitable media. Here front solutions are characteristic features of very slow diffusive receptors which can adapt only though the kinetics between their two states. Pulse solutions, however, behave very differently. These solutions, known in the literature as autosolitons [25], have the characteristic property that the region of excitation gets smaller with the excitability of the system. Depending on parameter ϵ controlling the excitability by continuous turn over of a controller variable, these solutions can form either stationary standing solutions or traveling waves of self-sustained structures. These receptors being the source of the coupling between the activator and the controller variables, the recruitment followed by the adaptation of these receptors in the regions of high excitation is crucial for the structural stability of expanding ring solutions which can transform into interacting spots. These instabilities have been previously studied in Refs. [30–32,47,50] for the exact Gray-Scott model in the asymptotic regime of a very large inhibitor diffusion length. In our model, these solutions appear in the regime of almost equal diffusion lengths for the activator and the inhibitor.

Receptor diffusion determines also the experimental signatures of the model for nascent structures [17,51,52]. First, our model can be used to investigate mechano-sensitivity as receptor recruitment is a central process in the early events of mechano-transduction. The use of biosensors has shown space and time modulation of signaling [53], a consequence of integrin activation, and this modulation amounts to taking different effective excitability parameters ϵ defined in (10). As seen in experiments, this leads to different self-organized structures. In the model, this parameter is controlled by an effective rate of disassembly τ [cf. (5)], with the property that signaling platforms are less active if they are down-regulated fast, so that ϵ decreases with increasing τ. Using this parameter, our model correlates the shape, the size and and the intensity of nascent adhesive structures with the rule that strongly activated structures have small spatial dimensions [54]. Second, our model shows that there exist two kinds of traveling waves in excitable media depending on whether receptors diffuse or not. In general, receptor diffusion slows down traveling waves and lead to stationary structures. In a typical numerical simulation, rosettes expand at a speed 1 activator diffusion length per minute, a value consistent with the observations. Expanding rosettes do not necessarily annihilate as in canonical models reviewed in Ref. [2], and more complex behaviors are possible. For podosomes, live cell imaging of rosettes shows that they can fuse, or annihilate, or granulate into spots which disappear. Our model demonstrates that adaptation and regulation of receptors have a major influence on interacting localized structures. Third, our model goes one step beyond conventional temporal signaling models and suggests that both the spatial and temporal activities of signaling components are crucial. It correlates characteristic times and length scales with shape dynamics, which may be useful for experiments probing shape responses to local photoablation [55].

ACKNOWLEDGMENTS

We thank A. Boudaoud, V. Lorman and A. Parmegiani for useful comments on a first version of the paper and A. Dupont for careful reading and suggestions. The Dislin library [56] was used in this work for figure preparation and movie presentation [49]. The group belongs to the CNRS consortium CellTiss. This work was supported by the ANR program PIRIbio and LNCC (équipe labelisée). M.R.B. and O.D. contributed equally to this work.

APPENDIX A: REDUCTION TO DIMENSIONLESS EQUATIONS

To define the parameter space of Fig. 2, it is useful to simplify the model by introducing dimensionless variables. Table I gives the appropriate change of variables where

$$n_0 = n_\infty \frac{K_e}{1+K_e} \ll n_\infty \tag{A1}$$

since K_e is small.

In the fast adaptive limit of integrin receptors, the equation of motions are therefore written in their dimensionless form as

$$\tilde{\epsilon} d\tilde{u}/d\tilde{t} = \frac{\tilde{\epsilon}}{d}\Delta\tilde{u} - \tilde{b}\tilde{u} + \tilde{v}e^{\tilde{u}}, \tag{A2}$$

$$d\tilde{v}/d\tilde{t} = \Delta\tilde{v} + \tilde{h}(1-\tilde{v}) - \tilde{v}e^{\tilde{u}}. \tag{A3}$$

To find the fixed point $(\tilde{u}_h, \tilde{v}_h)$ of the associated homogeneous system, we solve

$$\frac{\tilde{h}}{\tilde{b}} = \tilde{u}_h(\tilde{h}e^{-\tilde{u}_h} + 1) \tag{A4}$$

with $\tilde{v}_h = b\tilde{u}_h e^{-\tilde{u}_h}$. This shows that $(\tilde{h}, \tilde{h}/\tilde{b})$ are the natural parameters. Graphical analysis of (A4) gives the parameter space of Fig. 2. From Eqs. (A2) and (A3), we find that $\tilde{\epsilon}$ sets

TABLE I. Normalized parameters in the limit of slow and fast adaptation.

	$\tilde{u}$	$\tilde{v}$	$\tilde{h}$	$\tilde{b}$	$\tilde{\epsilon}$	$\tilde{t}$
Case a	βu	v/v_c	h/n_∞	$b/(n_\infty v_c \beta)$	$\epsilon/(\beta v_c)$	t/n_∞
Case b	βu	v/v_c	h/n_0	$b/(n_0 v_c \beta)$	$\epsilon/(\beta v_c)$	t/n_0

the ratio of two characteristic time scales. For typical values of parameters used in this paper, $\tilde{\epsilon}$ is a small number so that the activator u is fast with respect to the slow inhibitor v.

APPENDIX B: RELATIONSHIP WITH THE GRAY-SCOTT MODEL IN THE FAST-ADAPTIVE REGIME

To relate our model with the Gray-Scott model, it is instructive to substitute $e^{\tilde{u}}$ by $\tilde{u}^2$ in (A2) and (A3). After appropriate time and space rescaling, this gives

$$\alpha \frac{du}{dt} = \mu^2 \Delta u - u + Avu^2, \tag{B1}$$

$$\frac{dv}{dt} = (1 - v) - vu^2 \tag{B2}$$

with $\alpha = \tilde{\epsilon}\tilde{h}/\tilde{b}$, $\mu = \sqrt{\tilde{\epsilon}\tilde{h}/(\tilde{b}\tilde{d})}$, $A = \sqrt{\tilde{h}}/\tilde{b}$. The two parameters α and μ are the ratio for the characteristic time and length scales, respectively, for the activator and inhibitor. When K_e is small, one finds $\tilde{h} \gg 1$ with $\tilde{h}/\tilde{b}$ fixed, so that the homogeneous fixed point and the relevant time and length scales agree for both models in this limit. The parameter A couples the activator and the inhibitor, and the rescaling made to obtain Eqs. (B1) and (B2) is possible only for the square nonlinearity of the Gray-Scott model. For $A < 2$, the Gray-Scott has only one fixed point with null clines intersecting on the $u = 0$ axis. The natural smallness of our parameter $\tilde{\epsilon}$ corresponds to the well-studied limit $\alpha \approx \mu \ll 1$ with A small where self-replication instabilities for large A, oscillatory instabilities for small α and competition instabilities for very small μ have been studied in Refs. [29–32,50,57]. According to Ref. [29] the characteristic speed of traveling waves in the Gray-Scott model is set by the product $A\alpha^{-1/2}$, which is much larger than the dimensional parameter $\sqrt{D_u b/\epsilon}$ and the characteristic speed observed when receptor adaptation is not immediate.

[1] B. N. Kholodenko, J. F. Hancock, and W. Kolch, Nat. Rev. Mol. Cell Biol. **11**, 414 (2010).
[2] J. Allard and A. Mogilner, Curr. Opin. Cell Biol. **25**, 107 (2013).
[3] R. Buccione, J. D. Orth, and M. A. McNiven, Nat. Rev. Mol. Cell Biol. **5**, 647 (2004).
[4] S. Linder, Trends Cell Biol. **17**, 107 (2007).
[5] D. A. Murphy and S. A. Courtneidge, Nat. Rev. Mol. Cell Biol. **12**, 413 (2011).
[6] O. Destaing, M. R. Block, E. Planus, and C. Albiges-Rizo, Curr. Opin. Cell Biol. **23**, 597 (2011).
[7] H. Schachtner, S. D. J. Calaminus, S. G. Thomas, and L. M. Machesky, Cytoskeleton (Hoboken) **70**, 572 (2013).
[8] O. Destaing, C. Petropoulos, and C. Albiges-Rizo, Cell Adhesion Migration **8**, 256 (2014).
[9] R. O. Hynes, Cell **110**, 673 (2002).
[10] H. Yamaguchi and T. Oikawa, Oncotarget **1**, 320 (2010).
[11] D. Hoshino, K. M. Branch, and A. M. Weaver, J. Cell Sci. **126**, 2979 (2013).
[12] C. Luxenburg, D. Geblinger, E. Klein, K. Anderson, D. Hanein, B. Geiger, and L. Addadi, PLoS ONE **2**, e179 (2007).
[13] C. Badowski, G. Pawlak, A. Grichine, A. Chabadel, C. Oddou, P. Jurdic, M. Pfaff, C. Albiges-Rizo, and M. R. Block, Mol. Biol. Cell **19**, 633 (2008).
[14] T. Oikawa, T. Itoh, and T. Takenawa, J. Cell Biol. **182**, 157 (2008).
[15] O. Destaing, E. Planus, D. Bouvard, C. Oddou, C. Badowski, V. Bossy, A. Raducanu, B. Fourcade, C. Albiges-Rizo, and M. R. Block, Mol. Biol. Cell **21**, 4108 (2010).
[16] Y.-R. Pan, C.-L. Chen, and H.-C. Chen, J. Cell Biol. **195**, 113 (2011).
[17] C.-H. Yu, N. B. M. Rafiq, A. Krishnasamy, K. L. Hartman, G. E. Jones, A. D. Bershadsky, and M. P. Sheetz, Cell Rep. **5**, 1456 (2013).
[18] A. J. Koch and H. Meinhardt, Rev. Mod. Phys. **66**, 1481 (1994).
[19] J. Murray, *Mathematical Biology* (Springer-Verlag, Berlin, 1989).
[20] Y. Mori, A. Jilkine, and L. Edelstein-Keshet, Biophys. J. **94**, 3684 (2008).
[21] O. Ali, C. Albigès-Rizo, M. R. Block, and B. Fourcade, Phys. Biol. **6**, 25010 (2009).
[22] S. Whitelam, T. Bretschneider, and N. J. Burroughs, Phys. Rev. Lett. **102**, 198103 (2009).
[23] O. Ali, H. Guillou, O. Destaing, C. Albigès-Rizo, M. R. Block, and B. Fourcade, Biophys. J. **100**, 2595 (2011).
[24] E. Bernitt, C. G. Koh, N. Gov, and H.-G. Döbereiner, PLoS ONE **10**, 1 (2015).
[25] B. Kerner and V. V. Osipov, Sov. Phys. Usp. **32**, 101 (1989).
[26] T. Ohta and H. Nakazawa, Phys. Rev. A **45**, 5504 (1992).
[27] B. N. Vasiev, Phys. Lett. A **323**, 194 (2004).
[28] Krischer and Mikhailov, Phys. Rev. Lett. **73**, 3165 (1994).
[29] C. B. Muratov and V. V. Osipov, arXiv:patt-sol/9804001v4 (2002).
[30] C. B. Muratov and V. Osipov, SIAM J. Appl. Math. **62**, 1463 (2002).
[31] D. S. Morgan and T. J. Kaper, Physica D **192**, 33 (2004).
[32] T. Kolokolnikov and J. Wei, Eur. J. Appl. Math. **16**, 201 (2005).
[33] J. Pearson, Science **261**, 189 (1993).
[34] S. Kondo and T. Miura, Science **329**, 1616 (2010).
[35] V. Martel, C. Racaud-Sultan, S. Dupe, C. Marie, F. Paulhe, A. Galmiche, M. R. Block, and C. Albiges-Rizo, J. Biol. Chem. **276**, 21217 (2001).
[36] C. Cluzel, F. Saltel, J. Lussi, F. Paulhe, B. A. Imhof, and B. Wehrle-Haller, J. Cell Biol. **171**, 383 (2005).
[37] M. H. Ginsberg, A. Partridge, and S. J. Shattil, Curr. Opin. Cell Biol. **17**, 509 (2005).
[38] N. J. Anthis and I. D. Campbell, Trends Biochem. Sci. **36**, 191 (2011).
[39] G. Di Paolo, L. Pellegrini, K. Letinic, G. Cestra, R. Zoncu, S. Voronov, S. Chang, J. Guo, M. R. Wenk, and P. De Camilli, Nature (London) **420**, 85 (2002).
[40] K. Ling, R. L. Doughman, A. J. Firestone, M. W. Bunce, and R. A. Anderson, Nature (London) **420**, 89 (2002).
[41] K. Ling, N. J. Schill, M. P. Wagoner, Y. Sun, and R. A. Anderson, Trends Cell Biol. **16**, 276 (2006).
[42] K. R. Legate and R. Fässler, J. Cell Sci. **122**, 187 (2009).

[43] E. S. Welf, U. P. Naik, and B. A. Ogunnaike, Biophys. J. **103**, 1379 (2012).
[44] G. I. Bell, Science **200**, 618 (1978).
[45] S. McLaughlin, J. Wang, A. Gambhir, and D. Murray, Annu. Rev. Biophys. Biomol. Struct. **31**, 151 (2002).
[46] J. P. Xiong, T. Stehle, B. Diefenbach, R. Zhang, R. Dunker, D. L. Scott, A. Joachimiak, S. L. Goodman, and M. A. Arnaout, Science **294**, 339 (2001).
[47] M. Mimura and M. Nagayama, Chaos **7**, 817 (1997).
[48] B. Fourcade (unpublished).
[49] See Supplemental Material at http://link.aps.org/supplemental/10.1103/PhysRevE.92.042704 for movies to visualize the dynamics of solutions.
[50] C. B. Muratov and V. V. Osipov, Eur. Phys. J. B **22**, 213 (2001).
[51] C.-H. Yu, J. B. K. Law, M. Suryana, H. Y. Low, and M. P. Sheetz, Proc. Natl. Acad. Sci. U. S. A. **108**, 20585 (2011).
[52] H. Wolfenson, I. Lavelin, and B. Geiger, Dev. Cell **24**, 447 (2013).
[53] B. Liu, S. Lu, Y.-l. Hu, X. Liao, M. Ouyang, and Y. Wang, Sci. Rep. **4**, 7008 (2014).
[54] R. Zaidel-Bar, R. Milo, Z. Kam, and B. Geiger, J. Cell Sci. **120**, 137 (2007).
[55] O. Destaing (unplublished).
[56] The dislin library used in this work is available at http://www.dislin.de/.
[57] C. B. Muratov and V. V. Osipov, Phys. Rev. E **54**, 4860 (1996).